ACS APPLIED MATERIALS & INTERFACES

Research Article

www.acsami.org

Scalable Production of the Silicon–Tin Yin-Yang Hybrid Structure with Graphene Coating for High Performance Lithium-Ion Battery Anodes

Yan Jin,[†,∥] Yingling Tan,[†,∥] Xiaozhen Hu,[†] Bin Zhu,[†] Qinghui Zheng,[†] Zijiao Zhang,[‡] Guoying Zhu,[§] Qian Yu,[‡] Zhong Jin,[§] and Jia Zhu*[,†]

[†]National Laboratory of Solid State Microstructures, College of Engineering and Applied Sciences, and Collaborative Innovation Center of Advanced Microstructures, Nanjing University, Nanjing 210093, China

[‡]Center of Electron Microscopy and State Key Laboratory of Silicon Materials, Department of Materials Science & Engineering, Zhejiang University, Hangzhou 310027, China

[§]Key Laboratory of Mesoscopic Chemistry of MOE and Collaborative Innovation Center of Chemistry for Life Sciences, School of Chemistry and Chemical Engineering, Nanjing University, Nanjing 210093, China

Supporting Information

ABSTRACT: Alloy anodes possessed of high theoretical capacity show great potential for next-generation advanced lithium-ion battery. Even though huge volume change during lithium insertion and extraction leads to severe problems, such as pulverization and an unstable solid–electrolyte interphase (SEI), various nanostructures including nanoparticles, nanowires, and porous networks can address related challenges to improve electrochemical performance. However, the complex and expensive fabrication process hinders the widespread application of nanostructured alloy anodes, which generate an urgent demand of low-cost and scalable processes to fabricate building blocks with fine controls of size, morphology, and porosity. Here, we demonstrate a scalable and low-cost process to produce a porous yin-yang hybrid composite anode with graphene coating through high energy ball-milling and selective chemical etching. With void space to buffer the expansion, the produced functional electrodes demonstrate stable cycling performance of 910 mAh g^{-1} over 600 cycles at a rate of 0.5C for Si-graphene "yin" particles and 750 mAh g^{-1} over 300 cycles at 0.2C for Sn-graphene "yang" particles. Therefore, we open up a new approach to fabricate alloy anode materials at low-cost, low-energy consumption, and large scale. This type of porous silicon or tin composite with graphene coating can also potentially play a significant role in thermoelectrics and optoelectronics applications.

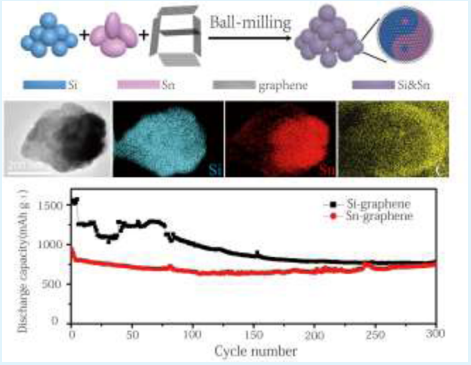

KEYWORDS: *silicon–tin, yin-yang, ball-milling, selective chemical etching, lithium-ion battery anode*

INTRODUCTION

The ever growing requirement of energy storage and electrical equipment has driven the increasing research efforts toward next-generation advanced rechargeable lithium-ion batteries (LIBs), especially high energy and power density electrode materials.[1−5] Alloy anodes possessed of high theoretical capacity show potential advantages. In the same main group of the periodic table of elements as the commercial anode of graphite, the silicon and tin element demonstrate high theoretical capacity of 4200 mAh g^{-1} and 994 mAh g^{-1} through binding 4.4 lithium ions of each alloy atom to form $Li_{4.4}Si$ and $Li_{4.4}Sn$ alloys, respectively.[6−9] However, huge lithium accommodation leads to ∼300% volume change for both Si and Sn alloys, resulting in severe problems, such as pulverization and unstable solid–electrolyte interphase (SEI) and generated capacity fading and limited cycle life.[10,11]

To address these failure problems, a wide range of material design concepts have been developed in the past decades. Mechanical fracture is avoided by decreasing the material feature size to the nanoscale, such as nanoparticle,[12−19] nanowire,[20−25] nanotube,[26−28] and porous network.[29−35] Besides, conformal graphene coating is another effective strategy with the following three advantages.[36−41] First, graphene is intrinsically highly electron conductive and ionic penetrating through defects, which can remain the electrochemical activity of fractured pieces. Second, the mechanically strong and flexible graphene layer can confine the inner alloy materials and preserve initial structures. Third, graphene can be used as an electrolyte-blocking layer because any possible

Received: January 9, 2017
Accepted: April 17, 2017
Published: April 17, 2017

DOI: 10.1021/acsami.7b00366
ACS Appl. Mater. Interfaces 2017, 9, 15388−15393

defects of graphene can be sealed by the SEI to prevent electrolyte infiltration through the conformal shell, which can provide a stable SEI layer on the outer graphene layer. Therefore, a conformal graphene-coated nanostructure alloy anode is expected to demonstrate stable cycling performance. However, the existing processes for producing graphene-coated alloy nanoparticle are still largely limited to a few expensive, complex, and energy-intensive processes, such as a high-temperature procedure for converting silicon precursors (such as silane) into a silicon nanoparticle, complex chemical synthesis with tin salt solution for Sn nanoparticle, and chemical vapor deposition with methane precursors and metal catalyst for graphene coating. In order to further enable widespread applications, a large-scale and low-cost process to fabricate these functional building blocks is urgently needed, which requires finely controlled morphology and porosity to enable high Coulombic efficiency and stable electrochemical performance.

Here, we demonstrate a low-cost, low-energy consumption and scalable method to fabricate two kinds of graphene-coated porous alloy anodes at the same time. Through high-energy ball-milling the mixture of low-grade silicon, metallic tin, and graphene, a yin-yang hybrid composite was obtained, in which silicon (yin part) and tin (yang part) homogeneously mix together within thin layers of graphene.[42] By selective chemical etching to remove the silicon or tin part, a porous silicon−graphene or porous tin−graphene composite can relieve the generated stress because of void space in the structure, which demonstrates a stable performance of 910 mAh g^{-1} over 600 cycles at a rate of 0.5C for Si−graphene "yin" particles and 750 mAh g^{-1} over 300 cycles at 0.2C for Sn−graphene "yang" particles. This type of porous silicon or tin composite with graphene coating derived from low-cost, low-energy consumption and large-scale synthesis is also beneficial for thermoelectrics and optoelectronics applications.

EXPERIMENTAL SECTION

2.1. Fabrication Processes of Porous Silicon−Graphene or Tin−Graphene Composites. 98% metallurgical-grade silicon, tin powder (325 mesh, Alfa Aesar), and graphene were used as received to prepare porous silicon−graphene or tin−graphene composites via a high-energy mechanical mill (HEMM) and selective chemical etching. First, metallurgical Si (~$1/kg) chock is used as the starting material and then is broken by a hammer into millimeter fragments. Next, metallurgical Si powder is obtained through a HEMM for 4 h at a speed of 750 r min^{-1}. Then a mixture of metallurgical Si powder, tin, and graphene with a weight ratio of 4.5:4.5:1 was ball-milled at a speed of 400 r min^{-1} for 4 h to form a hybrid composite, in which silicon (yin part) and tin (yang part) homogeneously mix together inside the graphene layer. The Si−Sn−graphene powder was then immersed in HCl or KOH solution for 15 min to selectively etch Sn or Si, respectively. The final porous silicon−graphene or porous tin−graphene composites were obtained from a series of continuous operations including centrifuge, washing three times with deionized water and ethanol, and drying in a vacuum oven at 80 °C for 8 h to prevent oxidation.

2.2. Material Characterizations. We applied scanning electron microscopy (Dual-beam FIB 235, FEI Strata) to characterize the morphology of the obtained composites. Transmission electron microscopy (JEM-200CX) is then used to further confirm the detailed structure. To distinguish the composition, the X-ray diffraction spectrum (Rigaku Ultima X-ray IV diffractometer) is employed, along with a Cu Ka 1° min^{-1}. Nitrogen sorption isotherms were acquired using a surface area and porosity analyzer (Tristar micromeritics) at −196 °C.

2.3. Electrochemical Testing. To test the electrochemical performance of the obtained anode composites, we prepared the anode on conductive current collectors (copper foil). The electrode slurry was made up of the received porous silicon−graphene or tin−graphene composite, CMC binder, and conductive additive of carbon black at weight ratio of 2:1:1. Then the slurry was spread on the current collector, and the electrode was obtained after drying in the vacuum oven for 12 h at 110 °C. We assembled the 2032 coin cell in the glovebox with O_2 and H_2O less than 0.1 ppm. Li metal foil was used as the counter electrode with Celgard 2250 as the separator. Electrolyte additive of 2 m% vinylene carbonate was added to the electrolyte containing 1.0 M LiPF6 in 1:1 vol/vol diethyl carbonate/ethylene carbonate (Guotai huarong Company) for much more stable cycling performance. LANHE CT2001A was employed to test galvanostatic cycling, and 0.01 V (vs Li/Li+) was the cutoff voltage for both Si and Sn alloy anode composites. The mass concerned in gravimetric capacity calculation includes alloy component and wrapped graphene layer. The theoretical capacity of Si and Sn is 4200 mAh g^{-1} and 994 mAh g^{-1}, which is the baseline for specific rate calculation. The average mass loading was 0.5−1 mg cm^{-2}. Cyclic voltammograms were performed in the range of 3−0.01 V along with a scanning rate of 0.1 mV s^{-1} on a CHI660E workstation (CH Instruments, Shanghai).

RESULTS AND DISCUSSION

The Si−Sn−graphene composite was prepared through ball-milling as illustrated in Figure 1a. The mixture of metallurgical Si powder, tin, and graphene with a weight ratio of 4.5:4.5:1 was ball-milled at a speed of 400 r min^{-1} to form a hybrid composite. Silicon and tin homogeneously mix together like a traditional Chinese yin-yang structure.[42] A ductile graphene layer was covered on the surface of the particle to enhance the electrical conductivities of structures and offer a stable interface layer for stabilizing SEI formation during electrochemical cycling. Scanning electron microscopy (SEM) and transmission electron microscopy (TEM) were used to characterize the morphology and detailed crystalline structure of the produced Si−Sn−graphene composite particles. Figure 1b shows typical hybrid particles with silicon and tin homogeneous dispersion and a graphene layer shell. We used TEM in Figure 1c to further confirm our structure. An about 10 nm thick graphene

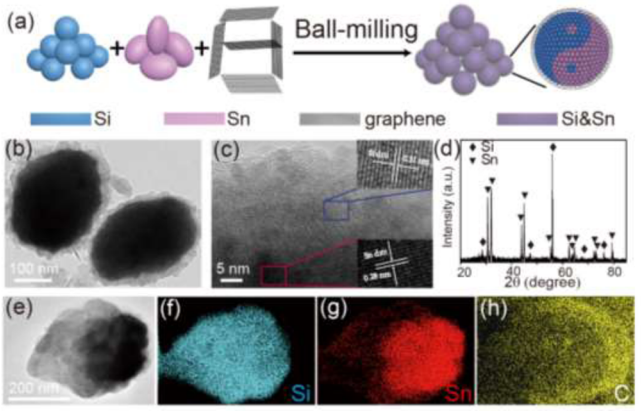

Figure 1. Fabrication processes and characterizations of Si−Sn−graphene composite particles. (a) Schematic of the fabrication process: blue silicon, rose red tin, and black graphene layer was ball-milled together to form the Si−Sn−graphene composite; (b) and (c) TEM images of Si−Sn−graphene particles at different magnifications; (d) XRD pattern of Si−Sn−graphene; (e) TEM image of the Si−Sn−graphene composite particle, and (f), (g), and (h) corresponding EDS elemental mappings of Si, Sn, and C, respectively.

DOI: 10.1021/acsami.7b00366
ACS Appl. Mater. Interfaces 2017, 9, 15388−15393

layer can be identified along the surface of the composite particle. Two kinds of lattice fringes with interplanar spacing of 0.31 and 0.28 nm are demonstrated in the inset high-resolution TEM in Figure 1c, which reflects the (111) plane of cubic silicon (marked blue rectangular frame) and the (101) plane of tetragonal tin (marked red rectangular frame). From the XRD pattern of the Si−Sn−graphene composite in Figure 1d, we can see typical peaks of Si (JCPDS #27−1402) and Sn (JCPDS #04−0673), consistent with the data of TEM. To fully figure out the element distribution inside a composite particle, electron dispersion spectroscopy mappings of the specific particle were shown in Figure 1e−1h. The Si element and Sn element uniformly distribute in the whole particle, which further confirmed the yin-yang integrated structure. The carbon element outlines the shape of the particle, proving there is a uniformly encapsulated graphene layer outside of the particles.

As we already know, Si and Sn alloy anodes suffer ∼300% volume change during electrochemical cycling, which leads to severe particle pulverization and an unstable SEI layer, resulting in fast capacity decay. In order to solve the problem, selective chemical etching was introduced to produce a porous anode. The obtained Si−Sn−graphene composite powder was immersed in HCl solution to dissolve Sn component, and the remaining silicon and graphene layer make up the porous silicon−graphene structure shown in Figure 2a. As depicted in the inset of Figure 2a, the rose red yang part in the yin−yang diagram turns empty because Sn is dissolved in HCl, and the blue yin component is left. In Figure 2b, the high-resolution TEM image exhibited a uniform graphene layer. The only lattice fringes left are the (111) plane of cubic silicon (blue marked rectangular frame) with basal distances of 0.31 nm.

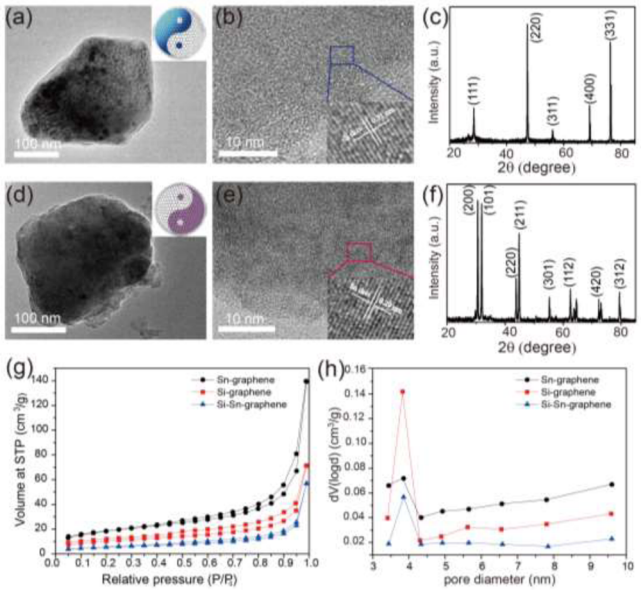

Figure 2. Characterizations of porous Si−graphene and Sn−graphene particles after selective chemical etching. (a) and (b) TEM images of porous Si−graphene particles at different magnifications. Inset schematic of (a): blue silicon and white void space in the graphene layer; (c) XRD pattern of porous Si−graphene; (d) and (e) TEM images of porous Sn−graphene particles at different magnifications. Inset schematic of (d): rose red tin and white void space in graphene layer; (f) XRD pattern of porous Sn−graphene; (g) and (h) nitrogen isotherm plots and pore volume distribution curves of Si−Sn−graphene, Si−graphene, and Sn−graphene particle samples.

Only the Si peak appears in XRD spectra in Figure 2c, which further confirms that Sn was totally removed by HCl acid etching to form a porous Si−graphene structure. 80 wt % silicon content in the composite is determined by thermal gravimetric (TG) analysis (Figure S3).

At the same time, if we change HCl to KOH solution, a complementary structure was obtained, as the Si component was dissolved in KOH solution and the porous Sn−graphene composite was left. Figure 2d−2f reveals the detailed structure and component information. Lattice fringes of the (101) plane of tetragonal tin (marked red rectangular frame) with basal distances of 0.29 nm presented in Figure 2d of the high-resolution TEM image and Sn peak in XRD spectra (Figure 2f) demonstrate that Sn was left in the remaining composite.

Moreover, we used nitrogen gas sorption measurements (Figure 2g and 2h) to study the distribution of pore size and surface area of the as-fabricated porous composites. The surface area is 37.01 and 66.41 $m^2\ g^{-1}$, which was calculated from the Brunauer−Emmett−Teller theory, for porous Si−graphene and Sn−graphene composites, respectively. It is reasonable that the Sn−graphene composite has larger surface area than Si−graphene. In the Si−Sn−graphene composite, even though the weight proportion of the Si and Sn composite is 1:1, the density of Si and Sn metal is 2.33 and 7.31 g cm^{-3}, which lead to different volume proportion in the particle. As we selectively dissolve the Si or Sn component to form porous structure, the remaining surface area of the Sn−graphene composite is larger as removed Si occupied more volume. The pore diameter of the porous Si−graphene and Sn−graphene is ∼4 nm, which was calculated by the Barrett−Joyner−Halenda method from the adsorption branch.

As demonstrated above, based on the highly scalable ball-milling and selective chemical etching process, we can produce porous Si−graphene and Sn−graphene composites, which are perceived as promising building blocks of an advanced lithium-ion battery anode for several important reasons. First, a huge volume change resulting from lithium insertion and extraction can be accommodated by void space in the obtained porous structures, which can suppress severe particle pulverization and unstable SEI layer. Second, a ductile graphene layer was covered on the surface of the particle to enhance electrical conductivity and offer a stable interface layer for stabilizing SEI formation during electrochemical cycling. Therefore, porous Si−graphene and Sn−graphene composites can offer high capacity, good rate performance, as well high CE, ideal for the next generation LIBs.

Figure 3 presents the electrochemical performance of a porous Si−graphene composite. As demonstrated in Figure 3a, cyclic voltammograms of the first three cycles were conducted in the voltage range of 0−3 V at a scanning rate of 0.1 mV s^{-1}. In the first cathodic cycle, a peak appears around 0 V, which indicates that the beginning silicon is crystal. This result matches well with XRD data in Figure 2c. Afterward, in the first anodic scan, reaction happens at ∼0.35 V and ∼0.53 V, which are the typical peaks for amorphous silicon and suggested that the crystal silicon was turned amorphous in the initial lithiation stage. The crystal structure transformation is further evidenced by a new characteristic peak of amorphous Si presented at ∼0.20 V in the subsequent cathodic scans. In addition, the long stable plateau in the charge−discharge curve of the initial cycle presented in Figure S1 is consistent with other silicon nanostrucures.[12] Besides, rate performance is performed at different current densities. It is expected that the unique

DOI: 10.1021/acsami.7b00366
ACS Appl. Mater. Interfaces 2017, 9, 15388−15393

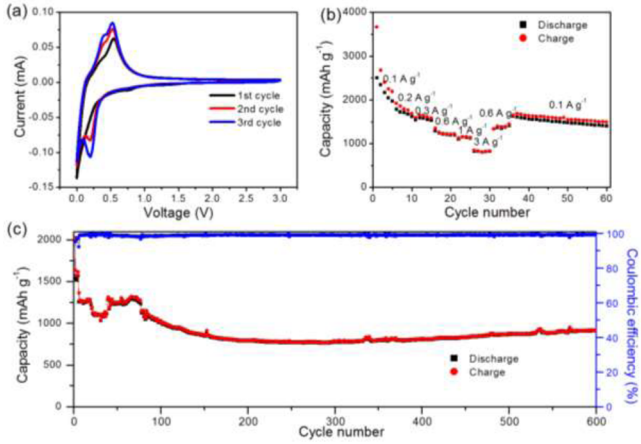

Figure 3. Electrochemical performance of a porous Si−graphene composite. (a) Cyclic voltammetry curves of the first three cycles. (b) Cycling performance at different current densities from 100 mA g^{-1} to 3000 mA g^{-1}. (c) Charge−discharge cycling test of the porous Si−graphene composite.

structure of void space among the porous structure and uniform graphene layer on the outside surface can be attributed to a stable performance. As presented in Figure 3b, the remaining discharge capacity is 2500 mAh g^{-1} when the conducted current density is 100 mA g^{-1}, and the capacity can maintain above 800 mAh g^{-1} with the applied current of 3000 mA g^{-1}. Long-term cycling performance, presented in Figure 3c, is tested under current density of 200 mA g^{-1} for the first 5 cycles, and conducted current density is increased to 2000 mA g^{-1} for the later cycling. In the initial cycle, the discharge capacity can reach 1536 mAh g^{-1} with 75.82% initial Coulombic efficiency of the obtained porous Si−graphene composite. The loss of first reversible capacities is largely due to irreversible decomposition of electrolyte to form the SEI layer on anode particles. Long-term cycling performance demonstrated the stable charge capacity above 900 mA h g^{-1} after 600 cycles.

At the same time, we studied the electrochemical properties of the Sn−graphene composite in Figure 4. Figure 4a shows the

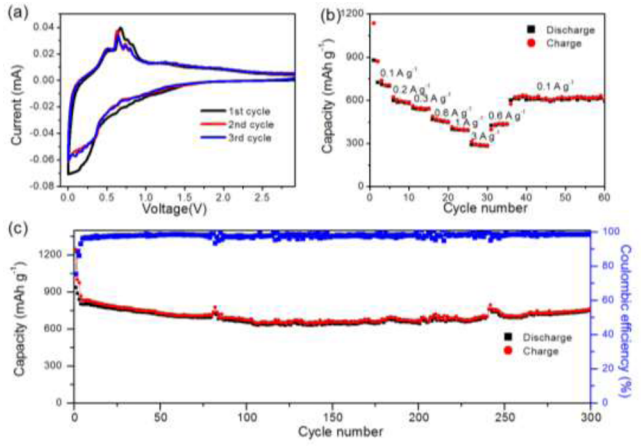

Figure 4. Electrochemical performance of a porous Sn−graphene composite. (a) Cyclic voltammetry curves of the first three cycles. (b) Cycling performance at different current densities from 100 mA g^{-1} to 3000 mA g^{-1}. (c) Charge−discharge cycling test of a porous Sn−graphene composite.

cyclic voltammetry (CV) of the first three scanning cycles, indicating electrochemical reactivity. There is a broad reduction band at 0.7 V in the first cathodic curve, which disappeared in the later cycles. It is the characteristic of irreversible electrolyte decomposition at the anode particle surface to form an SEI layer.[28] In the delithiation procedure, typical redox peaks at 0.55, 0.67, 0.76, and 0.82 V appear.[13] All main peaks are reproducible, which confirms the reversibility of the steady-state process. Figure S2 displays the voltage profiles of porous Sn−graphene composites at current density of 200 mA g^{-1}, similar to the typical characteristics of a Sn electrode.[14] In the initial cycle, the discharge and charge capacity are 1103 and 813 mAh g^{-1}, respectively. Rate performance with current densities ranging from 100 mA g^{-1} to 3000 mA g^{-1}, presented in Figure 4b, can further evaluate electrochemical performance. The capacity retention is 300 mAh g^{-1} at 3000 mA g^{-1} and returned to above 600 mAh g^{-1} upon changing current density to 100 mA g^{-1}. The long cycling test presented in Figure 4c indicated that after 300 cycles electrochemical cycling at 200 mA g^{-1}, the specific capacity is still maintained at 750 mAh g^{-1}. Because the formation of a thick SEI layer on the electrode surface at the first discharge can result in large initial capacity loss of the Sn−graphene composite electrode, the initial Coulombic efficiency of Sn−graphene are 75.29%. Therefore, it is confirmed that the porous Sn structure wrapped by a graphene layer can enable stable cycling and rate performance.

CONCLUSION

In summary, we demonstrate a scalable method to fabricate a graphene-coated porous yin-yang hybrid composite anode through high energy ball milling and selective chemical etching at large scale and low cost. The obtained porous silicon−graphene or porous tin−graphene composite can relieve the generated stress with void space in the structure, which demonstrates a stable performance of 910 mAh g^{-1} over 600 cycles at a rate of 0.5C for Si−graphene "yin" particles and 750 mAh g^{-1} over 300 cycles at 0.2C for Sn−graphene "yang" particles. This type of porous silicon or tin graphene composite from low-cost processes can also be employed in many other energy applications such as thermoelectrics and solar energy.

ASSOCIATED CONTENT

Supporting Information

The Supporting Information is available free of charge on the ACS Publications website at DOI: 10.1021/acsami.7b00366.

Voltage profiles for the porous Si−graphene composite and Sn−graphene composite; TG curve of Si−graphene composite (PDF)

AUTHOR INFORMATION

Corresponding Author

*E-mail: jiazhu@nju.edu.cn (J. Z.).

ORCID

Yan Jin: 0000-0003-0811-0100

Zhong Jin: 0000-0001-8860-8579

Author Contributions

‖Y.J. and Y.T. contributed equally to this work.

Notes

The authors declare no competing financial interest.

DOI: 10.1021/acsami.7b00366
ACS Appl. Mater. Interfaces 2017, 9, 15388−15393

■ ACKNOWLEDGMENTS

We acknowledge the microfabrication center of National Laboratory of Solid State Microstructures (NLSSM) for technique support. This work is jointly supported by the State Key Program for Basic Research of China (No. 2015CB659300), National Natural Science Foundation of China (Nos. 11621091, 11574143), Natural Science Foundation of Jiangsu Province (Nos. BK20150056, BK20160630), Postdoctoral Science Foundation of China (No.2016M601774), the Project Funded by the Priority Academic Program Development of Jiangsu Higher Education Institutions (PAPD), and the Fundamental Research Funds for the Central Universities.

■ REFERENCES

(1) Dunn, B.; Kamath, H.; Tarascon, J. M. Electrical Energy Storage for the Grid: A Battery of Choices. *Science* **2011**, *334*, 928−935.
(2) Goodenough, J. B.; Kim, Y. Challenges for Rechargeable Li Batteries. *Chem. Mater.* **2010**, *22*, 587−603.
(3) Tarascon, J. M.; Armand, M. Issues and Challenges Facing Rechargeable Lithium Batteries. *Nature* **2001**, *414*, 359−367.
(4) Arico, A. S.; Bruce, P.; Scrosati, B.; Tarascon, J. M.; van Schalkwijk, W. Nanostructured Materials for Advanced Energy Conversion and Storage Devices. *Nat. Mater.* **2005**, *4*, 366−377.
(5) Armand, M.; Tarascon, J. M. Building Better Batteries. *Nature* **2008**, *451*, 652−657.
(6) Winter, M.; Besenhard, J. O. Electrochemical Lithiation of Tin and Tin-Based Intermetallics and Composites. *Electrochim. Acta* **1999**, *45*, 31−50.
(7) Park, C. M.; Kim, J. H.; Kim, H.; Sohn, H. J. Li-Alloy Based Anode Materials for Li Secondary Batteries. *Chem. Soc. Rev.* **2010**, *39*, 3115−3141.
(8) Li, H.; Wang, Z. X.; Chen, L. Q.; Huang, X. J. Research on Advanced Materials for Li-Ion Batteries. *Adv. Mater.* **2009**, *21*, 4593−4607.
(9) Ji, L. W.; Lin, Z.; Alcoutlabi, M.; Zhang, X. W. Recent Developments in Nanostructured Anode Materials for Rechargeable Lithium-Ion Batteries. *Energy Environ. Sci.* **2011**, *4*, 2682−2699.
(10) Wu, H.; Cui, Y. Designing Nanostructured Si Anodes for High Energy Lithium Ion Batteries. *Nano Today* **2012**, *7*, 414−429.
(11) Kasavajjula, U.; Wang, C. S.; Appleby, A. J. Nano- and Bulk-Silicon-Based Insertion Anodes for Lithium-Ion Secondary Cells. *J. Power Sources* **2007**, *163*, 1003−1039.
(12) Yao, Y.; McDowell, M. T.; Ryu, I.; Wu, H.; Liu, N.; Hu, L.; Nix, W. D.; Cui, Y. Interconnected Silicon Hollow Nanospheres for Lithium-Ion Battery Anodes with Long Cycle Life. *Nano Lett.* **2011**, *11*, 2949−2954.
(13) Liu, N.; Wu, H.; McDowell, M. T.; Yao, Y.; Wang, C.; Cui, Y. A Yolk-Shell Design for Stabilized and Scalable Li-Ion Battery Alloy Anodes. *Nano Lett.* **2012**, *12*, 3315−3321.
(14) Jiao, Y.; Han, D.; Ding, Y.; Zhang, X.; Guo, G.; Hu, J.; Yang, D.; Dong, A. Fabrication of Three-Dimensionally Interconnected Nanoparticle Superlattices and Their Lithium-Ion Storage Properties. *Nat. Commun.* **2015**, *6*, 6420.
(15) Liu, N.; Lu, Z.; Zhao, J.; McDowell, M. T.; Lee, H. W.; Zhao, W.; Cui, Y. A Pomegranate-Inspired Nanoscale Design for Large-Volume-Change Lithium Battery Anodes. *Nat. Nanotechnol.* **2014**, *9*, 187−92.
(16) Zhu, B.; Jin, Y.; Tan, Y. L.; Zong, L. Q.; Hu, Y.; Chen, L.; Chen, Y. B.; Zhang, Q.; Zhu, J. Scalable Production of Si Nanoparticles Directly from Low Grade Sources for Lithium-Ion Battery Anode. *Nano Lett.* **2015**, *15*, 5750−5754.
(17) Zhu, Z. Q.; Wang, S. W.; Du, J.; Jin, Q.; Zhang, T. R.; Cheng, F. Y.; Chen, J. Ultrasmall Sn Nanoparticles Embedded in Nitrogen-Doped Porous Carbon As High-Performance Anode for Lithium-Ion Batteries. *Nano Lett.* **2014**, *14*, 153−157.
(18) Yu, Y.; Gu, L.; Wang, C.; Dhanabalan, A.; van Aken, P. A.; Maier, J. Encapsulation of Sn@Carbon Nanoparticles in Bamboo-like Hollow Carbon Nanofibers as an Anode Material in Lithium-Based Batteries. *Angew. Chem., Int. Ed.* **2009**, *48*, 6485−6489.
(19) Wang, G. X.; Wang, B.; Wang, X. L.; Park, J.; Dou, S. X.; Ahn, H.; Kim, K. Sn/Graphene Nanocomposite with 3d Architecture for Enhanced Reversible Lithium Storage in Lithium Ion Batteries. *J. Mater. Chem.* **2009**, *19*, 8378−8384.
(20) Guan, C.; Wang, X.; Zhang, Q.; Fan, Z.; Zhang, H.; Fan, H. J. Highly Stable and Reversible Lithium Storage in SnO_2 Nanowires Surface Coated with a Uniform Hollow Shell by Atomic Layer Deposition. *Nano Lett.* **2014**, *14*, 4852−4858.
(21) Cui, L. F.; Ruffo, R.; Chan, C. K.; Peng, H. L.; Cui, Y. Crystalline-Amorphous Core-Shell Silicon Nanowires for High Capacity and High Current Battery Electrodes. *Nano Lett.* **2009**, *9*, 491−495.
(22) Chan, C. K.; Peng, H.; Liu, G.; McIlwrath, K.; Zhang, X. F.; Huggins, R. A.; Cui, Y. High-Performance Lithium Battery Anodes Using Silicon Nanowires. *Nat. Nanotechnol.* **2008**, *3*, 31−35.
(23) Xiao, Y.; Hao, D.; Chen, H. X.; Gong, Z. L.; Yang, Y. Economical Synthesis and Promotion of the Electrochemical Performance of Silicon Nanowires as Anode Material in Li-Ion Batteries. *ACS Appl. Mater. Interfaces* **2013**, *5*, 1681−1687.
(24) Chen, H. X.; Xiao, Y.; Wang, L.; Yang, Y. Silicon Nanowires Coated with Copper Layer as Anode Materials for Lithium-Ion Batteries. *J. Power Sources* **2011**, *196*, 6657−6662.
(25) Xu, W. W.; Zhao, K. N.; Niu, C. J.; Zhang, L.; Cai, Z. Y.; Han, C. H.; He, L.; Shen, T.; Yan, M. Y.; Qu, L. B.; Mai, L. Q. Heterogeneous Branched Core-Shell SnO_2-Pani Nanorod Arrays with Mechanical Integrity and Three Dimentional Electron Transport for Lithium Batteries. *Nano Energy* **2014**, *8*, 196−204.
(26) Wu, H.; Chan, G.; Choi, J. W.; Ryu, I.; Yao, Y.; McDowell, M. T.; Lee, S. W.; Jackson, A.; Yang, Y.; Hu, L. B.; Cui, Y. Stable Cycling of Double-Walled Silicon Nanotube Battery Anodes through Solid-Electrolyte Interphase Control. *Nat. Nanotechnol.* **2012**, *7*, 310−315.
(27) Park, M. H.; Kim, M. G.; Joo, J.; Kim, K.; Kim, J.; Ahn, S.; Cui, Y.; Cho, J. Silicon Nanotube Battery Anodes. *Nano Lett.* **2009**, *9*, 3844−3847.
(28) Yu, Y.; Gu, L.; Zhu, C. B.; van Aken, P. A.; Maier, J. Tin Nanoparticles Encapsulated in Porous Multichannel Carbon Microtubes: Preparation by Single-Nozzle Electrospinning and Application as Anode Material for High-Performance Li-Based Batteries. *J. Am. Chem. Soc.* **2009**, *131*, 15984−11985.
(29) Jung, D. S.; Ryou, M. H.; Sung, Y. J.; Park, S. B.; Choi, J. W. Recycling Rice Husks for High-Capacity Lithium Battery Anodes. *Proc. Natl. Acad. Sci. U. S. A.* **2013**, *110*, 12229−12234.
(30) Li, X.; Gu, M.; Hu, S.; Kennard, R.; Yan, P.; Chen, X.; Wang, C.; Sailor, M. J.; Zhang, J. G.; Liu, J. Mesoporous Silicon Sponge as an Anti-Pulverization Structure for High-Performance Lithium-Ion Battery Anodes. *Nat. Commun.* **2014**, *5*, 4105.
(31) Ge, M.; Lu, Y.; Ercius, P.; Rong, J.; Fang, X.; Mecklenburg, M.; Zhou, C. Large-Scale Fabrication, 3d Tomography, and Lithium-Ion Battery Application of Porous Silicon. *Nano Lett.* **2014**, *14*, 261−268.
(32) Kim, H.; Han, B.; Choo, J.; Cho, J. Three-Dimensional Porous Silicon Particles for Use in High-Performance Lithium Secondary Batteries. *Angew. Chem., Int. Ed.* **2008**, *47*, 10151−10154.
(33) Magasinski, A.; Dixon, P.; Hertzberg, B.; Kvit, A.; Ayala, J.; Yushin, G. High-Performance Lithium-Ion Anodes using a Hierarchical Bottom-up Approach. *Nat. Mater.* **2010**, *9*, 353−358.
(34) Jia, H. P.; Gao, P. F.; Yang, J.; Wang, J. L.; Nuli, Y. N.; Yang, Z. Novel Three-Dimensional Mesoporous Silicon for High Power Lithium-Ion Battery Anode Material. *Adv. Energy Mater.* **2011**, *1*, 1036−1039.
(35) Han, X.; Chen, H. X.; Liu, J. J.; Liu, H. H.; Wang, P.; Huang, K.; Li, C.; Chen, S. Y.; Yang, Y. A Peanut Shell Inspired Scalable Synthesis of Three-Dimensional Carbon Coated Porous Silicon Particles as an Anode for Lithium-Ion Batteries. *Electrochim. Acta* **2015**, *156*, 11−19.
(36) Han, X.; Chen, H. X.; Zhang, Z. Q.; Huang, D. L.; Xu, J. F.; Li, C.; Chen, S. Y.; Yang, Y. Carbon-Coated Si Micrometer Particles

DOI: 10.1021/acsami.7b00366
ACS Appl. Mater. Interfaces 2017, 9, 15388−15393

Binding to Reduced Graphene Oxide for a Stable High-Capacity Lithium-Ion Battery Anode. *J. Mater. Chem. A* **2016**, *4*, 17757−17763.
(37) Li, Y.; Yan, K.; Lee, H.-W.; Lu, Z.; Liu, N.; Cui, Y. Growth of Conformal Graphene Cages on Micrometre-Sized Silicon Particles as Stable Battery Anodes. *Nat. Energy* **2016**, *1*, 15029.
(38) Luo, J.; Zhao, X.; Wu, J.; Jang, H. D.; Kung, H. H.; Huang, J. Crumpled Graphene-Encapsulated Si Nanoparticles for Lithium Ion Battery Anodes. *J. Phys. Chem. Lett.* **2012**, *3*, 1824−9.
(39) Mao, S.; Wen, Z.; Kim, H.; Lu, G.; Hurley, P.; Chen, J. A General Approach to One-Pot Fabrication of Crumpled Graphene-Based Nanohybrids for Energy Applications. *ACS Nano* **2012**, *6*, 7505−13.
(40) Yang, S.; Feng, X.; Ivanovici, S.; Mullen, K. Fabrication of Graphene-Encapsulated Oxide Nanoparticles: Towards High-Performance Anode Materials for Lithium Storage. *Angew. Chem., Int. Ed.* **2010**, *49*, 8408−11.
(41) Zhao, Y.; Feng, J.; Liu, X.; Wang, F.; Wang, L.; Shi, C.; Huang, L.; Feng, X.; Chen, X.; Xu, L.; Yan, M.; Zhang, Q.; Bai, X.; Wu, H.; Mai, L. Self-Adaptive Strain-Relaxation Optimization for High-Energy Lithium Storage Material Through Crumpling of Graphene. *Nat. Commun.* **2014**, *5*, 4565.
(42) Li, J. *Research on the Spreading of Taiji Culture*; World Acad Union-World Acad Press: Liverpool, 2010.

DOI: 10.1021/acsami.7b00366
ACS Appl. Mater. Interfaces 2017, 9, 15388−15393